RESEARCH ARTICLE | OCTOBER 15 2025

On the ambient conditions crystal structure of $AgSbTe_2$

Baihong Sun ; Sergei Grazhdannikov ; Muhamed Dawod; Lunhua He ; Jiazheng Hao; Thomas Meier ; Yansun Yao ; Yaron Amouyal ; Elissaios Stavrou

Appl. Phys. Lett. 127, 151905 (2025)
https://doi.org/10.1063/5.0293705

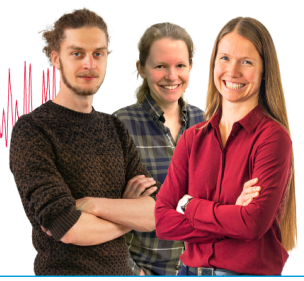

Applied Physics Letters ARTICLE pubs.aip.org/aip/apl

On the ambient conditions crystal structure of $AgSbTe_2$

Cite as: Appl. Phys. Lett. **127**, 151905 (2025); doi: 10.1063/5.0293705
Submitted: 29 July 2025 · Accepted: 26 September 2025 ·
Published Online: 15 October 2025

Baihong Sun,[1,2] Sergei Grazhdannikov,[2] Muhamed Dawod,[2] Lunhua He,[3,4,5] Jiazheng Hao,[4,6] Thomas Meier,[7,a)] Yansun Yao,[8,b)] Yaron Amouyal,[2,c)] and Elissaios Stavrou[1,2,9,d)]

AFFILIATIONS

[1]Materials Science and Engineering Department, Guangdong Technion-Israel Institute of Technology, Shantou 515063, China
[2]Department of Materials Science and Engineering, Technion-Israel Institute of Technology, Haifa 3200003, Israel
[3]Beijing National Laboratory for Condensed Matter Physics, Institute of Physics, Chinese Academy of Sciences, Beijing 100190, People's Republic of China
[4]Spallation Neutron Source Science Center, Dongguan 523803, People's Republic of China
[5]Songshan Lake Materials Laboratory, Dongguan 523808, People's Republic of China
[6]Institute of High Energy Physics, Chinese Academy of Sciences, Beijing 100049, People's Republic of China
[7]Shanghai Key Laboratory MFree, Institute for Shanghai Advanced Research in Physical Sciences, Pudong, Shanghai 201203, China
[8]Department of Physics and Engineering Physics, University of Saskatchewan Saskatoon, Saskatoon, Saskatchewan S7N 5E2, Canada
[9]Guangdong Provincial Key Laboratory of Materials and Technologies for Energy Conversion, Guangdong Technion-Israel Institute of Technology, Shantou 515063, China

[a)]**Electronic mail:** thomas.meier@hpstar.ac.cn
[b)]**Electronic mail:** yansun.yao@usask.ca
[c)]**Electronic mail:** amouyal@technion.ac.il
[d)]**Author to whom correspondence should be addressed:** elissaios.stavrou@gtiit.edu.cn

ABSTRACT

We present a combined x-ray and neutron diffraction, Raman spectroscopy, and ^{121}Sb nuclear magnetic resonance (NMR) experimental study of $AgSbTe_2$, supported by first-principles calculations aiming to elucidate its crystal structure. While diffraction methods cannot unambiguously identify the structure, Raman and NMR data, together with electric field gradient calculations, strongly support a rhombohedral $R\bar{3}m$ phase. Moreover, the agreement between experimental and calculated Raman spectra further corroborates this result, resolving the 60-year old debate about the exact crystal structure of the $AgSbTe_2$ compound.

The global growing demands for energy consumption and the accompanying environmental issues have forced the scientific community to find solutions to overcome the energy crisis and the development of sustainable and environmentally friendly energy resources has become critical.[1] In this context, the application of thermoelectric (TE) materials, which can directly convert energy from heat to electricity and vice versa, offers a promising approach to overcome present challenges. $AgSbTe_2$, a ternary chalcogenide TE material, stands out mainly due to its exceptionally low thermal conductivity (0.5–0.7 $Wm^{-1}K^{-1}$[2–4]) and its exceptionally narrow bandgap of 7.6 meV.[5] Recently, it has gained significant attention for achieving a high figure of merit (ZT) of approximately 2.6 at 573 K through cadmium doping.[6]

Accurate determination of its crystal structure is of critical importance for relevant theoretical calculations aiming to elucidate and tune its thermal and electrical transport properties followed by its high TE performance. However, its crystal structure at room temperature (RT) has been the subject of a long debate. Initially, it was considered to have a cubic $Fm\bar{3}m$ disordered NaCl-type partial solid solution structure.[7] In this crystal structure, Ag and Sb occupy the 4a Wyckoff positions (Na-site) with 50% occupancy. This solid solution arrangement was challenged by Quarez *et al.*[8] and three ordered structures, with

space groups $Pm\bar{3}m$, $P4/mmm$ and $R\bar{3}m$ (α-$NaFeO_2$-type), have been proposed as the ones that can best index the corresponding single-crystal x-ray diffraction (XRD) results.

Subsequent first-principles calculations[4] suggested that the ordered $Fd\bar{3}m$ ($D4$) crystal structure has lower energy compared to the structures identified by Quarez *et al.* However, in the same study, rhombohedral $R\bar{3}m$ ($L1_1$) was found to have practically degenerate energy with the $D4$ structure. Indeed, the negligible energy difference between the $D4$ and $L1_1$ structures was confirmed by later first-principles calculations.[9–11] Further first-principles studies of the temperature-dependent Helmholtz free energies of the cubic, tetragonal, and rhombohedral polymorphs indicate slight differences between these three values around RT, making the identification of the stable structure inconclusive.[12–14] Therefore, the exact crystal structure of $AgSbTe_2$ remains an open question. Moreover, different synthesis paths may lead to the coexistence of multiple compounds/phases (e.g., $AgSbTe_2$+Ag_2Te), as also observed in this study.

In this study, our goal is to accurately determine the crystal structure of $AgSbTe_2$ based on the previously proposed crystal structures $Fm\bar{3}m$, $Pm\bar{3}m$, $P4/mmm$, $L1_1$, and $D4$. We used concomitant XRD, neutron diffraction (ND), Raman spectroscopy, and solid-state nuclear magnetic resonance (NMR) experimental probes combined with first-principles density functional theory (DFT) calculations of the corresponding Raman spectra. Both diffraction techniques are unable to provide a definitive structural determination. On the other hand, Raman as well as NMR spectroscopy offer conclusive evidence for the rhombohedral $L1_1$ crystal structure.

$AgSbTe_2$ specimens were synthesized from high-purity raw materials, including silver (Ag, 99.999%, Alfa Aesar) granules, antimony (Sb, 99.999%, Alfa Aesar) granules, and tellurium (Te, 99.99%, Strem Chemicals) broken ingots. The raw materials were mixed in a molar ratio of 1:1:2 (Ag:Sb:Te), resulting in a total ingot mass of 20 g. The mixture was loaded into quartz ampules, which were evacuated to 5×10^{-5} Torr residual pressure and sealed. The sealed ampules were annealed to 1000 °C in a programmable vertical tube furnace, where their molten content was mixed three times during a 32-h soaking period. Afterward, the ampules were cooled by quenching in ice-water to obtain $AgSbTe_2$ ingots, which were further ground into fine powders sieved with a 56 μm mesh. The microstructure and compositional characterization of the samples was carried out using a Zeiss® Ultra Plus high-resolution scanning electron microscope, as well as the FEI Quanta 200 SEM equipped with a 10 mm^2 active area Oxford® INCA X-sight energy-dispersive x-ray spectroscopy (EDS) detector. More details about the microstructure and compositional characterization of the samples are provided in the supplementary material, see text and Figs. S1–S3.

Powder XRD measurements were performed using the Cu K α_1 ($\lambda = 1.5406$ Å) x-ray line (Rigaku MiniFlex). Powder ND was performed using the general-purpose powder diffractometer (GPPD) located at the China Spallation Neutron Source (CSNS). The GPPD is a time-of-flight (TOF) diffractometer with a neutron bandwidth of 4.8 Å, providing a maximum resolution of Δ d/d = 0.15%. The neutron pattern data in this study were acquired from three different banks of GPPD: 150°, 90°, and 30°, corresponding to the central solid angles of the detector. The d-space ranges were 0.05–2.7, 0.06–4.3, and 0.12–28.11 Å, respectively.[15,16] The sample under investigation was loaded into a 9 mm diameter TiZr can and all measurements were performed at RT.

Raman studies were performed using a custom-made confocal micro-Raman system with the 660 nm line of a solid-state laser for excitation in back scattering geometry. The laser probing spot dimension was $\approx 4\,\mu$m. Raman spectra were recorded with a spectral resolution of 2 cm^{-1} using a single-stage grating spectrograph equipped with a charge-coupled device (CCD) array detector. The laser power on specimens was kept below 0.2 mW, to avoid any laser-induced decomposition. Ultra-low-frequency solid-state notch filters allowed us to measure Raman spectra down to 10 cm^{-1}.[17]

NMR spectroscopy was conducted at 5.87 T (^{1}H frequency 250 MHz) using homebuilt probes. ^{121}Sb NMR powder spectra were recorded over $\pm$2 MHz around 59.83 MHz using frequency-stepped Hahn echoes[18] with Gaussian amplitude modulation. The transmitter frequency was incremented in 25 kHz steps, employing 70 μs pulses (40 kHz excitation bandwidth) at 0.4 W pulse power. With a 100 ms repetition time, the average pulse power was under 0.4 mW to minimize sample decomposition. Due to rapid spin coherence decay ($T_2^* < 5\,\mu$s), echo pulse separations were kept below 6 µs. The full spectrum was reconstructed from individual echo intensities vs carrier frequency. Electric field gradient calculations followed standard definitions of quadrupolar parameters.[19,20] Atomic positions near Sb nuclei were iterated for $Fm\bar{3}m$ and $R\bar{3}m$ structures with a 50 Å cutoff. On-the-fly checks ensured convergence of Cq and η. Spectral simulations of full quadrupolar powder patterns employed the contour analysis method of Hughes and Harris,[21] accounting for first- and second-order quadrupolar interactions. The line shape was convoluted with a Voigt profile (40 kHz Lorentzian and Gaussian components) to model natural linewidth effects.

Raman frequencies and intensities were calculated from first principles using the linear response pseudopotential plane wave approach within the framework of density functional perturbation theory.[22] Local density approximation[23] was applied, and Troullier–Martins norm-conserving pseudopotentials[24] were employed, using valence states of $4d^{10}\ 5s^1$, $5s^2\ 5p^3$, $5s^2\ 5p^4$ for Ag, Sb, and Te, respectively. Integration over the first Brillouin zone was performed using a $16 \times 16 \times 16$ Monkhorst–Pack mesh.[25] All calculations were carried out with the QUANTUM ESPRESSO package.[26,27] The basic concept involves evaluating changes in charge polarization induced by vibrational perturbations (zone-center phonon). The background theory and computational techniques have been described elsewhere.[22] More details about the theoretical Raman spectra calculations are provided in the supplementary material.

The experimental XRD pattern of this study, compared with the calculated (by using the POWDER CELL program[28] in this study) patterns of the corresponding previously suggested crystal structures,[4,7,8] is shown in Fig. 1. It is clear that powder XRD results cannot provide a conclusive answer to the exact crystal structure, in agreement with previous studies, since it can be fitted with any of the suggested crystal structures. The additional observed Bragg peaks, besides those associated with $AgSbTe_2$, in the experimental XRD pattern can be assigned to the β-Ag_2Te second phase,[29] see inset of Fig. 1. The precipitation of β-Ag_2Te was also observed in previous studies.[30,31]

Rietveld refinements, using the *GSAS − II* software,[32] were performed on the ND pattern, using the previously proposed crystal structures. The $Fm\bar{3}m$ structure was used in order to determine the volume fraction of the β-Ag_2Te, as shown in Fig. S4(a) of the supplementary material. The volume fractions of the $AgSbTe_2$ and the β-Ag_2Te

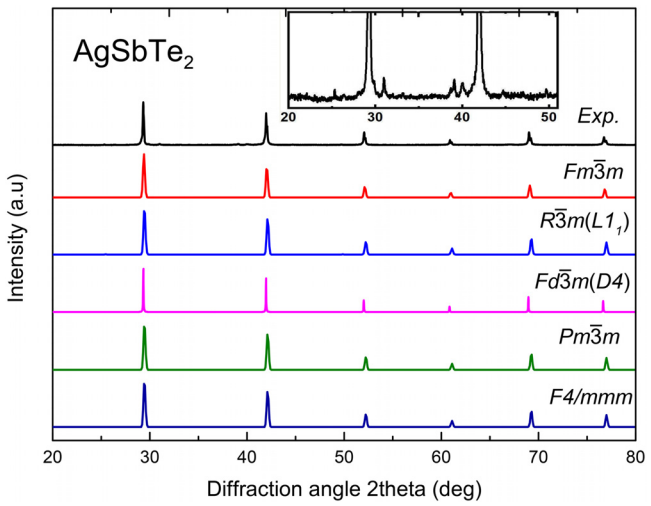

FIG. 1. Experimental XRD pattern of $AgSbTe_2$ (black) in comparison with the calculated patterns of the previously proposed crystal structures.[4,7,8] The inset showcases the Bragg peaks of the Ag_2Te impurity phase.

phases were determined to be 95.81% and 4.191%, respectively. Subsequently, the goodness of fit (GOF), the reduced χ^2 as well as R_w parameters for the various examined crystal structures were determined, see Figs. 2 and S4. These parameters were used as the criteria for assessing which structure provides a better fit. The refinements were performed by including β-Ag_2Te for each structural model and R_F was also used to compare the goodness of fit. In this case, the R_F values of $R\bar{3}m$ $AgSbTe_2$ show slightly superior goodness of fit compared to other structure. The corresponding results for the $Fm\bar{3}m$, $Fd\bar{3}m$ ($D4$), $R\bar{3}m$ ($L1_1$), $Pm\bar{3}m$ and $P4/mmm$ crystal structures are summarized in Table I. As in the case of powder XRD, powder ND results cannot definitively identify the crystal structure of $AgSbTe_2$. In

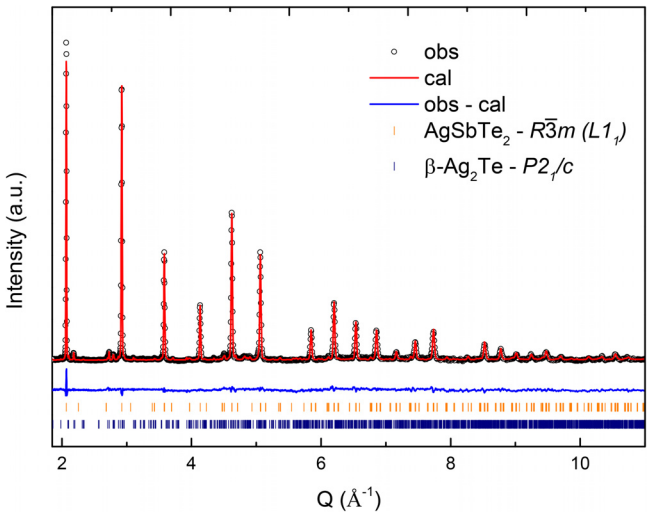

FIG. 2. Rietveld refinement of the experimental ND pattern of $AgSbTe_2$ using the $R\bar{3}m$ structural model. β-Ag_2Te ($P2_1/c$) was also included as a second phase.

fact, Rietveld refinement calculations for different preselected structures indicate similar results; see Table I. The shortcoming of ND is most probably associated with the similar coherent neutron scattering cross sections of Ag (4.407 b), Sb (3.9 b), and Te (4.23 b),[33] taking also into account the experimental limitation related to texture, instrument resolution, and the presence of β-Ag_2Te second phase.

According to group theory, the Raman active zone-center modes for the $L1_1$ crystal structure are $\tilde{\Gamma}_R = A_{1g} + E_g$.[34] Both modes are associated with the Te (6c) atom vibrations. This crystal structure is characterized by alternating Ag–Te–Sb–Te layers, perpendicular to the c-axis. For the A_{1g} mode, two adjacent Te layers vibrate rigidly against each other and parallel to the c-axis, while for the E_g mode, two adjacent Te layers vibrate against each other and perpendicular to the c-axis,[35,36] see Fig. S5 in the supplementary material. In contrast, all the other previously suggested/proposed crystal structures are Raman inactive.

Although the overall Raman intensity is low and the relevant Raman peaks are close to the Rayleigh line, the Raman spectrum of this study, see Fig. 3, clearly indicates the existence of two Raman active modes at 114.7 and 149.1 cm^{-1}. Furthermore, the relative intensities and frequencies are in fair agreement with those calculated for the $L1_1$ crystal structure of $AgSbTe_2$. The slight frequency mismatch ($< 20\%$) is quite reasonable in the case of Raman mode frequencies and is also affected by the specific approximation used in DFT calculations.[37] Moreover, the non-perfect stoichiometry of $AgSbTe_2$ effectively reduces the effective mass and may shift modes to higher frequencies. The agreement between intensities becomes even better after the subtraction of a simple baseline, reflecting the proximity to the Rayleigh line, see blue spectrum in Fig. 3. We attribute the apparent high intensity of the Rayleigh scattering line to the, effectively, metallic character of $AgSbTe_2$. Indeed, previous studies indicate that $AgSbTe_2$ is either a semimetal[38] or a very narrow bandgap ($E_g \approx 7.6$ meV, below the thermal energy at ambient conditions) semiconductor with a high number of thermally excited and high-mobility electrons.[5] In addition to the agreement between the experimental and calculated spectra, further evidence supports the assignment of the observed Raman modes originating from the $R\bar{3}m$ structure. Indeed, the overall Raman spectrum "shape" and mode frequencies fit well with those of other α-$NaFeO_2$-type structure compounds, such as $LiNiO_2$ and $NaCrS_2$,[35,39] considering the higher mass of Te compared to oxygen and sulfur.

The ability to probe short- and medium-range local atomic arrangements makes nuclear magnetic resonance (NMR) spectroscopy a promising tool for elucidating the structural candidates of $AgSbTe_2$. In particular, the quadrupole moment of nuclei with spin quantum number $I > \frac{1}{2}$ interacts with the surrounding charge distribution via the local electric field gradient (EFG).[40] This quadrupolar interaction provides valuable information about the local symmetry and can be used to differentiate between competing structural models.[19] To this end, EFG tensors in their principal axis system were calculated for both the rock salt-like $Fm\bar{3}m$ and the rhombohedral $R\bar{3}m$ structural candidates of $AgSbTe_2$.

Figure 4(a) shows the calculated values of the quadrupolar coupling constant C_q (in kHz) as a function of the cutoff distance from the antimony atoms for both the $Fm\bar{3}m$ and $R\bar{3}m$ structural models. As shown, C_q remains zero for the rock salt-like structure, indicating complete quenching of the quadrupolar interaction, whereas the rhombohedral structure yields coupling constants around 540 kHz,

TABLE I. Rietveld refinement results of ND patterns of $AgSbTe_2$ for various previously suggested crystal structures. The $Fm\bar{3}m+\beta$-Ag_2Te mixture was independently used in one of the refinements to determine the volume fraction of the secondary phase β-Ag_2Te and the volume fraction of β-Ag_2Te was fixed in the other structural model refinements.

Space group	a (Å)	c (Å)	Ag	Sb	Te	GOF	R-χ^2	R_{wp}	$R_F^{AgSbTe_2}$	$R_F^{\beta-Ag_2Te}$	β-Ag_2Te (%)
$Fm\bar{3}m+\beta$-Ag_2Te	6.077	⋯	4a	4a	4b	2.10	4.41	3.011	12.93	30.71	4.19
$R\bar{3}m(L1_1)+\beta$-Ag_2Te	4.295	21.076	3b	3a	6b	1.90	3.60	2.709	9.82	25.55	⋯
$Fd\bar{3}m$ $(D4)+\beta$-Ag_2Te	12.154	⋯	16c	16d	32e	2.83	7.99	4.149	13.70	40.58	⋯
$Pm\bar{3}m+\beta$-Ag_2Te	6.077	⋯	3c	1b, 3c	1a, 3d	2.01	4.05	2.957	12.33	34.39	⋯
$P4/mmm+\beta$-Ag_2Te	4.297	6.077	1c	1b	1a, 1d	2.04	4.15	3.005	12.71	34.48	⋯

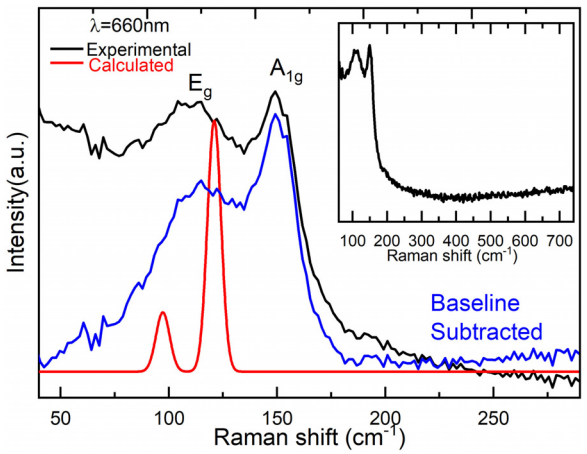

FIG. 3. Experimental Raman spectrum of $AgSbTe_2$ (black) in comparison with the calculated one (red). The blue spectrum is obtained after baseline subtraction from the experimental spectrum. The assignment of Raman mode symmetries is based on theoretical calculations. The inset shows an extended Raman shift range of the experimental spectrum.

consistent with an NMR spectrum governed by first-order quadrupolar interaction.[41] The experimental ^{121}Sb-NMR spectrum measured at a magnetic field strength of 5.87 T is shown in Fig. 4(b). The positions of the spectral singularities associated with the multiple-quantum satellite transitions, i.e., $||\pm5/2\rangle \leftrightarrow |\pm3/2\rangle$ and $|\pm3/2\rangle \leftrightarrow |\pm1/2\rangle$, indicate a quadrupolar coupling constant of $C_q^{(\mathrm{exp.})} = 529(20)$ kHz, in good agreement with the computed quadrupole coupling constant of the rhombohedral $R\bar{3}m$ structural candidate.

The XRD results indicate that all of the previously suggested structures can fit the experimental pattern adequately. The Rietveld refinements performed for the various structures also showed that there are negligible differences between structures.[8,42] However, no ND results have been reported for $AgSbTe_2$. Only one study reported ND measurements for $AgSbSe_2$, from which it was also not possible to determine cation ordering.[43] Our ND Rietveld refinements showed that the $L1_1$ structure exhibits a slightly better fit across all refinement criteria used in this study; see Table I. However, although these results point toward the $L1_1$ structure, the relative marginal differences preclude a definitive crystal structure determination.

According to the ND results, the sample contains ≈4% volume fraction of β-Ag_2Te as a secondary phase. In order to rule out the possibility that the observed Raman modes originate from this phase,

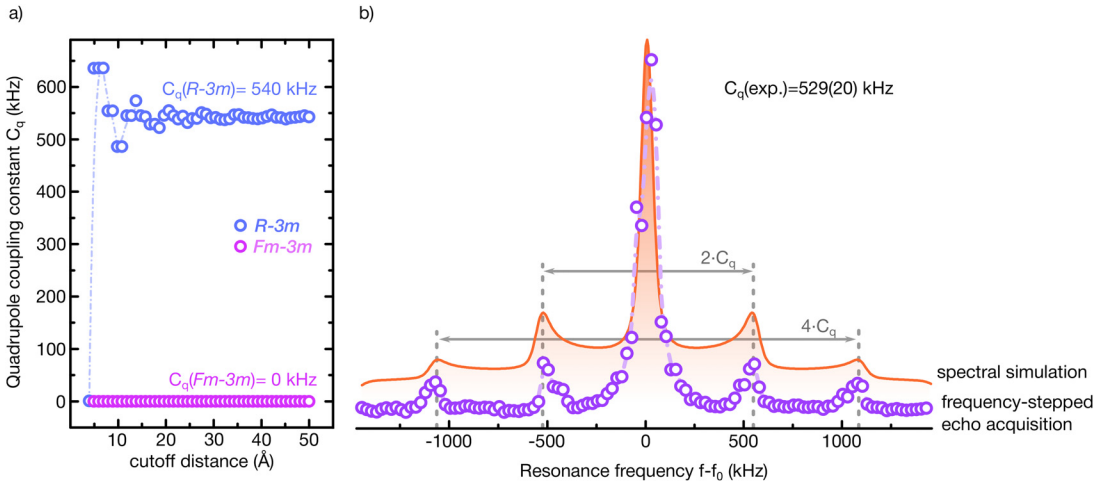

FIG. 4. (a) Numerical quadrupole coupling constants of ^{121}Sb in $Fm\bar{3}m$ and $R\bar{3}m$ structures as a function of cutoff distance (Å). Values of 0 and 540 kHz were computed for $Fm\bar{3}m$ and $R\bar{3}m$, respectively. The blue dashed line is a guide to the eye. (b) Frequency-stepped Hahn-echo acquisition recovered the $I = 5/2$ quadrupolar powder pattern (purple). The satellite Pake doublets indicate $C_q(\mathrm{exp.}) = 529(20)$ kHz. The orange line represents the corresponding spectral simulation. Spectral center f_0 was 59.83 MHz at 5.87 T.

albeit its very low amount, the experimental Raman spectrum was also compared to the Raman spectra of β-Ag_2Te from previous studies. The Raman spectrum of bulk polycrystalline β-Ag_2Te consists of two low-intensity broad bands at 111 and 134 cm^{-1} and a broader feature at about 80 cm^{-1}.[44] Also, the Raman spectrum of nano-β-Ag_2Te thin film exhibits a sharp peak at 152 cm^{-1} and a broad peak in the 220–315 cm^{-1} frequency range.[45] Another study found that the Raman spectrum of 3 nm thick β-Ag_2Te consists of Raman bands at 94.3, 121.8, and 141.9 cm^{-1}.[46]

In our study, only two bands were observed at frequencies clearly distinct from all previously reported ones for various forms of β-Ag_2Te. Moreover, according to previous Raman studies on Ag_2Te, it was established that a high intensity of the laser excitation can result in decomposition of $AgSbTe_2$ and the formation of TeO_2, with characteristic strong peaks at 360–400 and 660 cm^{-1}.[44] Such peaks are entirely absent in our experimental spectrum; see inset of Fig. 3. From the above discussion, together with the very low quantity of the β-Ag_2Te impurity, it can be accurately concluded that the observed Raman modes originate from pure Ag_2Te.

The study of the local charge symmetry surrounding antimony atoms, probed by the presented NMR experiments, demonstrated that a structurally isotropic rock salt-like $Fm\bar{3}m$ structure would result in a complete quenching of quadrupolar interaction and the observation of a single sharp resonance line, in clear contradiction to experimental observation. Indeed, recorded ^{121}Sb-NMR spectra show that the antimony spin system in $AgSbTe_2$ is subject to first order quadrupole interaction, strongly favoring the rhombohedral $R\bar{3}m$ structure, in good agreement with electric field gradient calculations. The existence of the Ag_2Te minority phase could either have no influence on the observed NMR spectra of $AgSbTe_2$, due to its low abundance, or parts of the $AgSbTe_2$ close to Ag_2Te could indeed sustain a disturbed EFG. However, the Sb quadrupole moment is very high and any stronger quadrupole interaction of the spin-5/2 system would lead to extremely broad signals below our detection limits. In fact, we scanned across a large frequency range around the main spectrum and no additional signals were observed. Thus, we conclude that the influence of Ag_2Te to be marginal on our NMR spectra.

Considering the combination of four experimental methods—x-ray diffraction, neutron diffraction, Raman spectroscopy, and NMR spectroscopy—together with *ab initio* DFT calculations, we have gathered conclusive evidence indicating the rhombohedral $R\bar{3}m$ crystal structure as the most likely structural candidate of the ternary thermoelectric chalcogenide $AgSbTe_2$. Although neutron diffraction refinements are compatible with the proposed model, conclusive structural identification arises from the excellent agreement between experimental and calculated Raman spectra. This assignment is further corroborated by NMR spectroscopy, which independently favors the rhombohedral $R\bar{3}m$ structure. Moreover, the determination of the $R\bar{3}m$ crystal structure using a bulk-probing technique, such as NMR, rules out the previously proposed existence of this phase as a minority nanodomain defect-like phase. Our study resolves a 60-years old debate about the crystal symmetry of $AgSbTe_2$ and will further facilitate relevant studies exploring and tuning its thermoelectric properties.

See the supplementary material for the following: Figure S1—presenting SEM-EDS elemental mapping of $AgSbTe_2$; Figure S2, representative energy-dispersive x-ray spectroscopy (EDS) spectra; Figure S3, a quasi-binary phase diagram of the Ag_2Te–Sb_2Te_3 system; Figure S4, Rietveld refinements of the experimental Neutron powder diffraction pattern; Figure S5, α-$NaFeO_2$-type crystal structure of $AgSbTe_2$ and Raman modes eigenvectors; Table S1, compositions of the $AgSbTe_2$ sample as determined using energy-dispersive x-ray spectroscopy; and additional theoretical details on the Raman spectra calculations.

The authors acknowledge receiving financial support from the Guangdong Technion—Israel Institute of Technology (Grant No. ST2100002), the Guangdong Provincial Key Laboratory of Materials and Technologies for Energy Conversion (Grant No. 2022B1212010007, Guangdong Department of Science and Technology), and the Natural Sciences and Engineering Research Council of Canada (NSERC). Y.A. gratefully acknowledges the generous support of the Pazy Research Foundation, under Grant No. 2032063. The authors acknowledge the use of beamtime at the GPPD granted by the China Spallation Neutron Source (Proposal ID: P1823122900035). This work was also supported by the National Key Research and Development Program of China (2022YFA1402301) and the National Science Foundation of China (42150101). T. Meier acknowledges receiving financial support from the Shanghai Key Laboratory Novel Extreme Condition Materials, China (No. 22dz2260800) and the Shanghai Science and Technology Committee, China (No. 22JC1410300).

AUTHOR DECLARATIONS

Conflict of Interest

The authors have no conflicts to disclose.

Author Contributions

Baihong Sun: Data curation (lead); Formal analysis (lead); Investigation (lead); Writing – original draft (equal); Writing – review & editing (equal). **Sergei Grazhdannikov:** Data curation (equal); Formal analysis (equal); Investigation (equal); Writing – review & editing (equal). **Muhamed Dawod:** Data curation (equal); Formal analysis (equal); Investigation (equal); Writing – review & editing (equal). **Lunhua He:** Resources (equal); Writing – review & editing (equal). **Jiazheng Hao:** Resources (equal); Writing – review & editing (equal). **Thomas Meier:** Data curation (equal); Formal analysis (equal); Investigation (lead); Methodology (equal); Writing – original draft (equal); Writing – review & editing (equal). **Yansun Yao:** Data curation (equal); Formal analysis (equal); Investigation (equal); Writing – original draft (equal); Writing – review & editing (equal). **Yaron Amouyal:** Funding acquisition (equal); Investigation (equal); Project administration (equal); Resources (lead); Supervision (lead); Validation (equal); Writing – review & editing (equal). **Elissaios Stavrou:** Conceptualization (lead); Funding acquisition (lead); Investigation (equal); Project administration (lead); Resources (lead); Supervision (lead); Writing – original draft (lead); Writing – review & editing (equal).

DATA AVAILABILITY

The data that support the findings of this study are available from the corresponding author upon reasonable request.

REFERENCES

[1]X.-L. Shi, J. Zou, and Z.-G. Chen, "Advanced thermoelectric design: From materials and structures to devices," Chem. Rev. **120**, 7399–7515 (2020).

[2]D. Morelli, V. Jovovic, and J. Heremans, "Intrinsically minimal thermal conductivity in cubic I-V-VI_2 semiconductors," Phys. Rev. Lett. **101**, 035901 (2008).
[3]C. E. Carlton, R. De Armas, J. Ma, A. F. May, O. Delaire, and Y. Shao-Horn, "Natural nanostructure and superlattice nanodomains in $AgSbTe_2$," J. Appl. Phys. **115**, 144903 (2014).
[4]K. Hoang, S. D. Mahanti, J. R. Salvador, and M. G. Kanatzidis, "Atomic ordering and gap formation in Ag-Sb-based ternary chalcogenides," Phys. Rev. Lett. **99**, 156403 (2007).
[5]V. Jovovic and J. P. Heremans, "Measurements of the energy band gap and valence band structure of $AgSbTe_2$," Phys. Rev. B **77**, 245204 (2008).
[6]S. Roychowdhury, T. Ghosh, R. Arora, M. Samanta, L. Xie, N. K. Singh, A. Soni, J. He, U. V. Waghmare, and K. Biswas, "Enhanced atomic ordering leads to high thermoelectric performance in $AgSbTe_2$," Science **371**, 722–727 (2021).
[7]S. Geller and J. H. Wernick, "Ternary semiconducting compounds with sodium chloride-like structure: $AgSbSe_2$, $AgSbTe_2$, $AgBiS_2$, $AgBiSe_2$," Acta Cryst. **12**, 46–54 (1959).
[8]E. Quarez, K.-F. Hsu, R. Pcionek, N. Frangis, E. K. Polychroniadis, and M. G. Kanatzidis, "Nanostructuring, compositional fluctuations, and atomic ordering in the thermoelectric materials $AgPb_mSbTe_{2+m}$. The myth of solid solutions," J. Am. Chem. Soc. **127**, 9177–9190 (2005).
[9]S. Barabash, V. Ozolins, and C. Wolverton, "First-principles theory of competing order types, phase separation, and phonon spectra in thermoelectric $AgPb_m$ $SbTe_{m+2}$ alloys," Phys. Rev. Lett. **101**, 155704 (2008).
[10]N. Rezaei, S. J. Hashemifar, and H. Akbarzadeh, "Thermoelectric properties of $AgSbTe_2$ from first-principles calculations," J. Appl. Phys. **116**, 103705 (2014).
[11]W. Szczypka and A. Koleżyński, "Theoretical studies of cation sublattice ordering in $AgSbTe_2$ and $AgSbSe_2$ – electron density topology and bonding properties," J. Alloys Compd. **732**, 293–299 (2018).
[12]Y. Amouyal, "On the role of lanthanum substitution defects in reducing lattice thermal conductivity of the $AgSbTe_2$ (P4/mmm) thermoelectric compound for energy conversion applications," Comput. Mater. Sci. **78**, 98–103 (2013).
[13]Y. Amouyal, "Reducing lattice thermal conductivity of the thermoelectric compound $AgSbTe_2$ (P4/mmm) by lanthanum substitution: Computational and experimental approaches," J. Electron. Mater. **43**, 3772–3779 (2014).
[14]Y. Amouyal, "Silver-antimony-telluride: From first-principles calculations to thermoelectric applications," in *Thermoelectrics for Power Generation*, edited by S. Skipidarov and M. Nikitin (IntechOpen, Rijeka, 2016), Chap. 7.
[15]L. He, S. Deng, F. Shen, J. Chen, H. Lu, Z. Tan, H. Zheng, J. Hao, D. Zhao, and Q. Ma, "The performance of general purpose powder diffractometer at CSNS," Nucl. Instrum. Methods Phys. Res. Sect. A **1054**, 168414 (2023).
[16]J. Hao, Z. Tan, H. Lu, S. Deng, F. Shen, D. Zhao, H. Zheng, Q. Ma, J. Chen, and L. He, "Residual stress measurement system of the general purpose powder diffractometer at CSNS," Nucl. Instrum. Methods Phys. Res. Sect. A **1055**, 168532 (2023).
[17]J. K. Hinton, S. M. Clarke, B. A. Steele, I.-F. W. Kuo, E. Greenberg, V. B. Prakapenka, M. Kunz, M. P. Kroonblawd, and E. Stavrou, "Effects of pressure on the structure and lattice dynamics of α-glycine: A combined experimental and theoretical study," CrystEngComm **21**, 4457–4464 (2019).
[18]E. L. Hahn, "Spin echoes," Phys. Rev. **80**, 580–594 (1950).
[19]P. P. Man, *Quadrupole Couplings in Nuclear Magnetic Resonance, General* (John Wiley & Sons, Ltd, 2006).
[20]J. Haase, "Magnetische Kernresonanz bei Quadrupolwechselwirkung in Festkoerpern," Ph.D. thesis (Leipzig University, 1995).
[21]C. E. Hughes and K. D. M. Harris, "Calculation of solid-state NMR lineshapes using contour analysis," Solid State Nucl. Magn. Reson. **80**, 7–13 (2016).
[22]S. Baroni, S. De Gironcoli, A. Dal Corso, and P. Giannozzi, "Phonons and related crystal properties from density-functional perturbation theory," Rev. Mod. Phys. **73**, 515 (2001).
[23]J. P. Perdew and Y. Wang, "Accurate and simple analytic representation of the electron-gas correlation energy," Phys. Rev. B **45**, 13244 (1992).
[24]N. Troullier and J. L. Martins, "Efficient pseudopotentials for plane-wave calculations," Phys. Rev. B **43**, 1993 (1991).
[25]H. J. Monkhorst and J. D. Pack, "Special points for Brillouin-zone integrations," Phys. Rev. B **13**, 5188 (1976).
[26]P. Giannozzi, S. Baroni, N. Bonini, M. Calandra, R. Car, C. Cavazzoni, D. Ceresoli, G. L. Chiarotti, M. Cococcioni, I. Dabo *et al.*, "QUANTUM ESPRESSO: A modular and open-source software project for quantum simulations of materials," J. Phys.: Condens. Matter. **21**, 395502 (2009).
[27]P. Giannozzi, O. Andreussi, T. Brumme, O. Bunau, M. B. Nardelli, M. Calandra, R. Car, C. Cavazzoni, D. Ceresoli, M. Cococcioni *et al.*, "Advanced capabilities for materials modelling with QUANTUM ESPRESSO," J. Phys.: Condens. Matter. **29**, 465901 (2017).
[28]W. Kraus and G. Nolze, "POWDER CELL–A program for the representation and manipulation of crystal structures and calculation of the resulting X-ray powder patterns," J. Appl. Crystallogr. **29**, 301–303 (1996).
[29]J. Schneider and H. Schulz, "X-ray powder diffraction of Ag_2Te at temperatures up to 1123 K," Z. Kristallogr.-Cryst. Mater. **203**, 1–16 (1993).
[30]Z. Hu, M. Yuan, W. Li, S. Wang, J. Li, J. Jiang, J. Shuai, and Y. Hou, "Enhanced thermoelectric performance in pristine $AgSbTe_2$ compound via rational design of Ag_2Te formation," Acta Mater. **290**, 120985 (2025).
[31]J. H. Kim, J. H. Yun, S. Cha, S. Byeon, J. Park, H. Jin, S. Kim, S.-J. Kim, J. Park, J. Jang *et al.*, "Enhancement of phase stability and thermoelectric performance of meta-stable $AgSbTe_2$ by thermal cycling process," Adv. Funct. Mater. **34**, 2404886 (2024).
[32]B. H. Toby and R. B. Von Dreele, "GSAS-II: The genesis of a modern open-source all purpose crystallography software package," J. Appl. Crystallogr. **46**, 544–549 (2013).
[33]V. F. Sears, "Neutron scattering lengths and cross sections," Neutron News **3**, 26–37 (1992).
[34]E. Kroumova, M. Aroyo, J. Perez-Mato, A. Kirov, C. Capillas, S. Ivantchev, and H. Wondratschek, "Bilbao crystallographic server: Useful databases and tools for phase-transition studies," Phase Transitions **76**, 155–170 (2003).
[35]P. Brüesch and C. Schüler, "Raman and infrared spectra of crystals with α-$NaFeO_2$ structure," J. Phys. Chem. Solids **32**, 1025–1038 (1971).
[36]A. Yelisseyev, P. Krinitsin, L. Isaenko, and S. Grazhdannikov, "Spectroscopic properties of nonlinear optical $LiGaTe_2$ crystal," Opt. Mater. **42**, 276–280 (2015).
[37]E. Stavrou, S. Lobanov, H. Dong, A. R. Oganov, V. B. Prakapenka, Z. Konôpková, and A. F. Goncharov, "Synthesis of ultra-incompressible sp^3-hybridized carbon nitride with 1:1 stoichiometry," Chem. Mater. **28**, 6925–6933 (2016).
[38]K. Hoang and S. D. Mahanti, "Atomic and electronic structures of I-V-VI_2 ternary chalcogenides," J. Sci. Adv. Mater. Devices **1**, 51–56 (2016).
[39]C. Julien, "Lithium intercalated compounds: Charge transfer and related properties," Mater. Sci. Eng.: R: Rep. **40**, 47–102 (2003).
[40]F. Holger Försterling, "Spin dynamics: Basics of nuclear magnetic resonance, second edition," Med. Phys. **37**, 406–407 (2010).
[41]D. Freude and J. Haase, *Quadrupole Effects in Solid-State Nuclear Magnetic Resonance* (Springer, 1993), pp. 1–90.
[42]Y.-H. Ko, M.-W. Oh, J. K. Lee, S.-D. Park, K.-J. Kim, and Y.-S. Choi, "Structural studies of $AgSbTe_2$ under pressure: Experimental and theoretical analyses," Curr. Appl. Phys. **14**, 1538–1542 (2014).
[43]K. Wojciechowski, M. Schmidt, J. Tobola, M. Koza, A. Olech, and R. Zybała, "Influence of doping on structural and thermoelectric properties of $AgSbSe_2$," J. Electron. Mater. **39**, 2053–2058 (2010).
[44]T. Milenov, T. Tenev, I. Miloushev, G. Avdeev, C.-W. Luo, and W.-C. Chou, "Preliminary studies of the Raman spectra of Ag_2Te and Ag_5Te_3," Opt. Quant. Electron. **46**, 573–580 (2014).
[45]M. Pandiaraman, N. Soundararajan, and R. Ganesan, "Optical studies of physically deposited nano-Ag_2Te thin films," in *Defect and Diffusion Forum* (Trans Tech Publications, 2011), Vol. 319, pp. 185–192.
[46]F. Sun, W. Hong, X. He, C. Jian, Q. Ju, Q. Cai, and W. Liu, "Synthesis of ultrathin topological insulator β-Ag_2Te and Ag_2Te/WSe_2-based high-performance photodetector," Small **19**, 2205353 (2023).